Int J Adv Manuf Technol (2015) 81:1055–1066
DOI 10.1007/s00170-015-7274-0

ORIGINAL ARTICLE

A novel model to predict U-bending springback and time-dependent springback for a HSLA steel plate

Hao-Jie Jiang [1,2] · **Hong-Liang Dai** [1,2]

Received: 23 January 2015 / Accepted: 4 May 2015 / Published online: 16 May 2015

Abstract In this paper, a novel model which considers initial strain related to the material's yielding stress, the combination of stretch and bending strain and isotropic hardening rule is introduced to predict U-bending springback and time-dependent springback behaviors for a high strength and low alloy (HSLA) steel plate. It is noteworthy that time-dependent springback is associated with plastic strain hardening for the HSLA steel plate. The results obtained from the performed analysis show that the hardening exponent, bending radius and thickness ratio, friction coefficient, and blank holder force have great influences on the springback angle and stress level. Based on this novel model, the prediction of HSLA steel plate's springback is done in the stage of tool design and hence, the accuracy of drawn part is increased.

Keywords Novel model · Time-dependent springback · U-bending · Springback angle · Stress level

1 Introduction

One of the main undesired phenomena that affect the accuracy of dimension and shape for the metallic-cold formed parts is the springback. On the plastic forming of metallic materials, it is necessary to measure, predict, and compensate for springback precisely and efficiently so that the final shape could be obtained precisely.

Different methods, such as analytical method, semi-analytical method, and finite element method, have been applied to predict the sheet springback. For eliminating springback error, Liu et al. [1] studied variable blank holder force in U-shaped part forming. Joining the tailor-welded strips by the laser welding process, Chang et al. [2] investigated the effect of different thickness combination on the springback. Cho et al. [3] employed the updated Lagrangian thermo-elastoplastic finite element method to a plane strain sheet metal U-bending process to aim at the numerical investigation on springback characteristics to the major process parameters. For understanding the mechanics of persistent anticlastic curvature which coincided with the phenomenon of draw-bend springback's sudden decline and its dependence on forming conditions, aluminum sheet strips of widths ranging from 12 to 50 mm were draw-bend tested by Wang et al. [4] with various sheet tensions and tool radii. According to the non-linear kinematic hardening theory of Lemaitre and Chaboche and Barlat89's yielding function, Zhang et al. [5] gave a sheet springback prediction. By finite element method, Yu and Lin [6] presented the effect of side pressure and stretch force on the dimension precision of aluminum profile rotary stretch-bending part. Based on Hill'48 yielding criterion and plane strain condition, Zhang et al. [7] proposed an analytical model for predicting sheet springback after U-bending. Based on the numerical simulation of the whole process, Gu et al. [8] revealed the springback mechanism and rule of thin-walled tube numerical controlling bending. By using the explicit implicit coupled finite element method, Li et al. [9] carried out numerical simulations for the multi-points forming process and the unloading springback to control and reduce springback. To analyze the unloading springback of sheet metal foils after micro-bending process, a constitutive model was

✉ Hong-Liang Dai
hldai520@sina.com

[1] State Key Laboratory of Advanced Design and Manufacturing for Vehicle Body, Hunan University, Changsha 410082, China

[2] Department of Engineering Mechanics, College of Mechanical and Vehicle Engineering, Hunan University, Changsha 410082, China

proposed by Liu et al. [10] based on the surface layer model by which the sheet foil was divided into surface layer and inner portions. Nanu and Brabie [11] established a model for prediction of springback parameters in the case of U-shaped stretch-bending process as a function of stresses distribution in the sheet thickness. Based on anisotropic hardening, Lee et al. [12] used a constitutive model in the finite element simulations of springback and compared its performance with that of conventional hardening laws. Using the Taguchi method, Kuo and Lin [13] investigated the springback of L-bending with a step in the die through simulation and experiments for AZ31 magnesium alloy sheets at different temperatures. Based on the classical elastoplastic theory and the characteristic of strain superposition, Zhao et al. [14] established the mechanical models of profile stretch-bending and obtained the universal analytic method of solving the plane stretch-bending springback for profile with any cross section. Performing experiments and finite element analyses of a U-shape forming test, Chongthairungruang et al. [15] compared the springback effect. Based on the advanced displacement adjustment method, Li et al. [16] developed a new geometrical springback compensation algorithm for automobile AHSS parts. Khan et al. [17] proposed an intelligent process model for predicting springback in the context of sheet metal forming, in particular, single-point incremental forming.

In terms of the time-dependent springback problems, Wagoner et al. [18, 19] simulated and measured the springback change of a part after forming. Zhu et al. [20] examined the time-dependent inelastic deformation of the aluminum alloy AA 5182-H19 during the manufacturing process and under in-service conditions. Based on previous springback measurement, Wang et al. [21] revealed that the specimen shapes of aluminum alloys could continue to change for long periods following forming and unloading. Lim et al. [22, 23] studied time-dependent springback behaviors of four advanced high-strength steels which measured and creep-simulated for various test conditions. E and Liu [24] explored the springback and time-dependent springback of 1Cr18Ni9Ti stainless steel tubes subject to bending. By applying viscoelastic/plastic constitutive law and utilizing a linear viscoelastic/plastic model, Park et al. [25] analyzed the time-dependent springback behavior of the aluminum alloy 6022-T4 sheet. However, the simple time-dependent springback of high-strength low-alloy (HSLA) steel plate in the case of U-bending process has rarely been reported.

Therefore, the investigation is carried out to explore the time-dependent springback of this shape's steel. A novel model is presented as an attempt to predict time-dependent springback and time-independent springback behaviors. In addition, the effects of such factors as hardening exponent, bending radius, and thickness ratio, normal anisotropy coefficient, friction coefficient, and blank holder force on springback angle and stress level of HSLA steel are investigated.

2 U-bending springback model of a HSLA steel plate

The U-bending parts are widely used in engineering practice, and of great research significances. Of course, the springback can be easily found during this U-bending process. The U-bending springback model of a HSLA steel plate is shown in Fig. 1a. Due to the symmetry behavior of geometry model and blank holder force, the bending springback model could be simplified and divided into following five zones (see Fig. 1b): (1) Zone (AB section) is in contact with bottom of blank holder and top die straight part; (2) Zone II (BC section) and zone IV (DE section) undergo the stretch-bending process, even zone II is in contact with the die corner, and zone IV in contact with the punch corner; (3) Zone III (CD section) sheet is reverse stretch-bending into the lateral arm after undergoing die corner's stretch-bending; (4) Zone V (EF section) is in contact with the bottom of the punch straight part. F_p and $\bar{l}$ are, respectively, the radii of punch and the die corner, and θ_1 and θ_2 are angles of zones IV and II, respectively. The following five hypotheses could be applied during the U-bending process of this model:

(1) The width of HSLA is far greater than the thickness, namely, the strain of width direction equals to zero (i.e., $\delta\theta_{\mathrm{IIIsw}}(^\circ)$).
(2) Kirchhoff's straight normal assumption is still feasible, i.e., the line perpendicular to middle-plane remains straight, which is still perpendicular to the middle-plane after deformation.
(3) Volume conservation is kept during stretch-bending process, i.e., $\delta\theta^{p}_{\mathrm{IIIsw}}(^\circ)$, where ε_θ and ε_r are, respectively, the tangential and transverse strains.

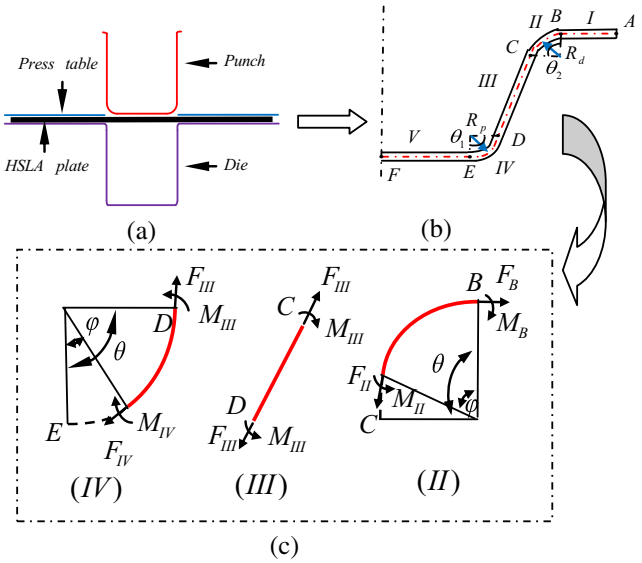

Fig. 1 **a** U-bending springback model of a HSLA steel plate. **b** Simplified U-bending part and considered zones. **c** Loading scheme for springback zones

(4) The transverse stress μ_d on thickness direction is neglected.
(5) The Bauschinger effect that occurs due to bending-unbending cycles in this model can be neglected (as the ratio between bending radius and sheet thickness is greater than 6). Thus, the isotropic hardening rule is considered in the bending-unbending process.

As the bending radius r is far greater than the thickness of HSLA steel plate t, shear strain ε_θ in the stretch-bending forming process can be represented as follows [26]

$$\varepsilon_\theta = \varepsilon_\theta^e + \varepsilon_\theta^p = \varepsilon_t + \frac{r-R_n}{R_n} \tag{1}$$

where, ε_θ^e is the tangential elastic strain, ε_θ^p denotes the tangential plastic strain, and ε_t represents the tensile strain. In Fig. 2a, r is the cylindrical coordinate, R_n is the bending radius of neutral layer, and the geometry of stretch and bent sheet, which can be seen in this figure. R_m is the bending radius of mid-plane and t is the thickness of HSLA steel plate. And F and M are the sheet tension and bending moment of stretch-bending cross section in Fig. 2a, respectively.

Considering the HSLA steel sheet is normal plastic anisotropy according to Hill's quadratic yield function [27], thus the relation between the plastic tangential stress σ_θ^p and the equivalent stress $\overline{\sigma}$ is [28]

$$\left|\sigma_\theta^p\right| = \frac{1+\overline{r}}{\sqrt{1+2\overline{r}}}\overline{\sigma} \tag{2}$$

where the sign "||" denoting the absolute value, $\overline{r}$ is the anisotropy coefficient (strain ratio between the length and thickness directions) on the thickness direction. Based on the Hollomon power function criterion [29, 30], equivalent stress $\overline{\sigma}$ can be expressed as

$$\overline{\sigma} = k(\varepsilon_0 + \overline{\varepsilon})^n \tag{3}$$

where k and n denote the hardening coefficient and hardening exponent, respectively. ε_0 is a material constant related to initial yielding stress, and $\overline{\varepsilon}$ is the equivalent strain.

Also, from Wagoner [28], it can be obtained that

$$\overline{\varepsilon} = \frac{1+\overline{r}}{\sqrt{1+2\overline{r}}}|\varepsilon_\theta| \tag{4}$$

Substituting Eqs. (5) and (6) into Eq. (3), yields

$$\left|\sigma_\theta^p\right| = kH[(\varepsilon_0 + H|\varepsilon_\theta|)]^n \tag{5}$$

where $H = \frac{1+\overline{r}}{\sqrt{1+2}}$, define c half the thickness of elastic region (seen in Fig. 2b), yields [26]

$$H = \frac{1+\overline{r}}{\sqrt{1+2\overline{r}}} \tag{6}$$

where E_1 is the Young's modulus under the plane strain condition and equals to $E/(1-\nu^2)$, E and ν are Young's modulus and Poisson's ratio of the plate, respectively, and σ_s is the initial yielding stress.

According to the material's stress-strain relationship, Eqs.(1) and (7), the distribution of tangential stress $\sigma_{l\theta}$(l=II, III, IV) on bending forming zones II, III, and IV throughout the sheet thickness can be

$$\sigma_{l\theta} = \begin{cases} \sigma_{l\theta}^e = E_1\left(\varepsilon_{lt} + \dfrac{r-R_{ln}}{R_{ln}}\right), & R_{ln}-c_l \le r \le R_{ln}+c_l \\ \sigma_{l\theta}^{p1} = -kH\left[\varepsilon_{l0} - H\left(\varepsilon_{lt} + \dfrac{r-R_{ln}}{R_{ln}}\right)\right]^n, & R_{li} \le r \le R_{ln}-c_l \\ \sigma_{l\theta}^{p2} = kH\left[\varepsilon_{l0} + H\left(\varepsilon_{lt} + \dfrac{r-R_{ln}}{R_{ln}}\right)\right]^n, & R_{ln}+c_l \le r \le R_{lo} \end{cases} \tag{7}$$

where all the symbols including a subscript l represents that it is on the lth bending forming zone, $\sigma_{l\theta}^e$, $\sigma_{l\theta}^{p1}$, and $\sigma_{l\theta}^{p2}$ denote tangential stresses of elastic and plastic regions, respectively. And R_{li} and R_{lo} are the inner and outer radii of the HSLA steel plate.

The blank holder forces per unit width, f_l, on bending forming zones II, III, and IV are defined, respectively, as

$$f_l = \frac{F_l}{b} = \int_{R_{li}}^{R_{ln}-c_l} \sigma_{l\theta}^{p1} dr + \int_{R_{ln}-c_l}^{R_{ln}+c_l} \sigma_{l\theta}^{e} dr + \int_{R_{ln}+c_l}^{R_{lo}} \sigma_{l\theta}^{p2} dr \tag{8}$$

where b is the width of the HSLA steel plate, sheet tensions F_l on bending forming zones II, III, and IV are given by the

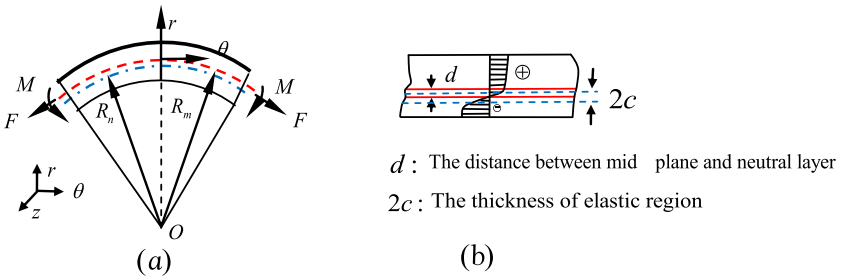

Fig. 2 **a** The scheme of sheet stretch-bending. **b** Stress distribution in the sheet thickness

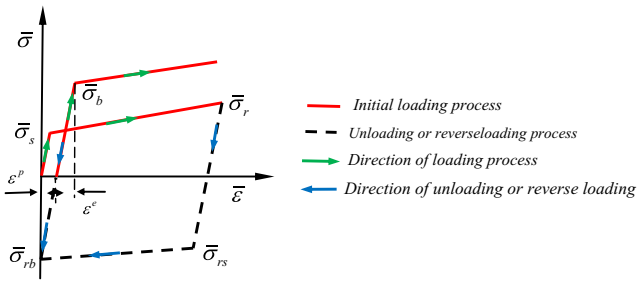

Fig. 3 The equivalent stress-strain relation of the isotropic hardening material model

following relations as [7, 11]$F_{\mathrm{II}} = F_B e^{\mu_d \phi}$, $F_{\mathrm{II}}=F_{\mathrm{III}}$, $F_{\mathrm{IV}} = F_{\mathrm{III}} e^{\mu_p(\phi-\theta)}$, $F_B=\mu_d F_p$ (9)where μ_p and μ_d represent the friction coefficients of punch and die, respectively. F_p is the blank holder force, ϕ denotes the angle describing position of any points on zones II and IV relative to points B and D (Fig. 1c). Based on the present model, the chosen angle $\phi=\pi/4$, the detailed force analysis process is shown in Fig. 1c.

3 Springback and stress analysis on zones II and IV

The bending moments $M_j(j=\mathrm{II},\ \mathrm{IV})$ of HSLA steel on zones II and IV are

$$M_j = \int_{R_{ji}}^{R_{jn}-c_j} \left(\sigma_{j\theta}^{p1}-\sigma_{jm\theta}\right)\left(r-R_{jm}\right)dr + \int_{R_{jn}-c_j}^{R_{jn}+c_j} \left(\sigma_{j\theta}^{e}-\sigma_{jm\theta}\right)\left(r-R_{jm}\right)dr + \int_{R_{jn}+c_j}^{R_{jo}} \left(\sigma_{j\theta}^{p2}-\sigma_{jm\theta}\right)\left(r-R_{jm}\right)dr = M_j^e + M_j^p \tag{10}$$

where all the symbols including a subscript j represents that it is on jth bending forming zone, M_j^e and M_j^p are the bending moments caused by tangential elastic strain and plastic strain hardening. For the stretch-bending process, the tangential stress on sheet middle surface caused by sheet tension, $\sigma_{jm\theta}$, yields

$$\sigma_{jm\theta} = \begin{cases} E_1\left(\varepsilon_{jt}+\dfrac{d_j}{R_{jn}}\right), & d_j \le c_j \\ kH\left[\varepsilon_{j0}+H\left(\varepsilon_{jt}+\dfrac{d_j}{R_{jn}}\right)\right]^n, & d_j > c_j \end{cases} \tag{11}$$

where $d_j(j=\mathrm{II},\ \mathrm{IV})$ is the distance between the mid-plane and neutral layer (seen in Fig. 2b), the bending moment caused by plastic strain hardening M_j^p on jth bending forming zone are

$$M_j^p = \int_{R_{ji}}^{R_{jn}-c_j} \left(\sigma_{j\theta}^{p1}-\sigma_{jm\theta}\right)\left(r-R_{jm}\right)dr + \int_{R_{jn}+c_j}^{R_{jo}} \left(\sigma_{j\theta}^{p2}-\sigma_{jm\theta}\right)\left(r-R_{jm}\right)dr \tag{12}$$

4 Springback and stress analysis in zone III

The zone III is the side arm part of U-bending for the HSLA steel, and the isotropic hardening rule is applied on the zone III as it undergoes a series of complex deformation history process, which includes the stretch-bending and reverse stretch-bending process. Although the zone III is of certain curvature before unloading for the existence of bending moment at cross section, the sheet metal can be considered a flat state in the process of U-bending forming as the gap between the punch and die is far less than the stretch depth.

For the isotropic hardening model, the equivalent stress-strain relationship of the HSLA steel plate's reverse-loading process is shown in Fig. 3, where ε_p and ε_e are plastic and elastic strains, respectively. The red solid line and the black dotted line represent the initial loading process and the unloading or reverse-loading process, respectively. The green arrow denotes the loading direction, and the blue arrow represents the unloading or reverse-loading direction. According to the isotropic hardening model, the following two key points need to be noted:

(1) The absolute values of hardening yielding stresses for that stretch stage, $\overline{\sigma}_{rb}$, and compression stage, $\overline{\sigma}_b$, are always the same.
(2) The yielding stress of reverse-loading stage, $\overline{\sigma}_{rs}$, equals to the unloading stress $\overline{\sigma}_r$.

For reverse-loading stage, the effective stress variation, which is based on isotropic hardening rule, $|\delta\overline{\sigma}_{\mathrm{III}\theta}|$, can be expressed as [7]

$$|\delta\overline{\sigma}_{\mathrm{III}\theta}| = \begin{cases} E_1\left|\delta\overline{\varepsilon}_{\mathrm{III}\theta}\right|, & \left|\delta\overline{\varepsilon}_{\mathrm{III}\theta}\right| \le 2\dfrac{|\overline{\sigma}_{\mathrm{III}r}|}{E_1} \\ k\left(\varepsilon_{\mathrm{III}0}+\left|\delta\overline{\varepsilon}_{\mathrm{III}\theta}\right|-2\dfrac{|\overline{\sigma}_{\mathrm{III}r}|}{E_1}\right)^n + 2|\overline{\sigma}_{\mathrm{III}r}|-\overline{\sigma}_s, & \left|\delta\overline{\varepsilon}_{\mathrm{III}\theta}\right| \ge 2\dfrac{|\overline{\sigma}_{\mathrm{III}r}|}{E_1} \end{cases} \tag{13}$$

Table 1 Chemical compositions of HSLA steel in weight percent (wt.%) [31]

C	Mn	Cu	Si	Cr	Mo	V	Ti	Al	Nb	Ni	P	S	Balance
0.08	1.40	<0.01	0.24	0.01	0.02	0.07	0.01	0.03	0.04	<0.01	0.005	0.005	Fe

Table 2 Principal mechanical property of HSLA steel

Yield strength, σ_s (MPa)	Hardening strength coefficient, k (MPa)	Hardening exponent, n (dimensionless)	Normal anisotropy coefficient, $\bar{r}$ (dimensionless)	Initial strain, ε_0 (dimensionless)
414	772	0.163	0.69	0.0012

where all the symbols including a subscript III represent that the discussed parameters are on the zone III, $\left|\delta\bar{\varepsilon}'_{\mathrm{III}\theta}\right|$ is the equivalent strain variation, and the tangential stress variation is also related to the material isotropic hardening rule during the complicated deformation history. According to Eqs. (3), (5), (7), and (15), by replacing the strain increment with the strain that resulted from reverse-bending process, the distribution of tangential stress variation through thickness of sheet, $|\delta\bar{\sigma}_{\mathrm{III}\theta}|$, can be written as

$$|\delta\bar{\sigma}_{III\theta}| = \begin{cases} E_1 H^2 \left|\varepsilon'_{\mathrm{III}t} + \dfrac{r-R_{\mathrm{III}n}}{R_{\mathrm{III}n}}\right|, & R_{\mathrm{III}n}-c_{\mathrm{III}} \le r \le R_{\mathrm{III}n}+c_{\mathrm{III}} \\ Hk\left(\varepsilon_{\mathrm{III}0} + H\left|\varepsilon'_{\mathrm{III}t} + \dfrac{r-R_{\mathrm{III}n}}{R_{\mathrm{III}n}}\right| - 2\dfrac{|\bar{\sigma}_{\mathrm{III}r}|}{E_1}\right)^n + 2H|\bar{\sigma}_{\mathrm{III}r}| - H\bar{\sigma}_s, & r = \text{others} \end{cases} \tag{14}$$

where $\varepsilon'_{\mathrm{III}t}$ is the strain caused by reverse stretch-bending process on the zone III, and

$$|\bar{\sigma}_{\mathrm{III}r}| = k\left[\varepsilon_{\mathrm{III}0} + H\left(\varepsilon'_{\mathrm{III}t} + \frac{r-R_{\mathrm{III}n}}{R_{\mathrm{III}n}}\right)\right]^n \tag{15}$$

The bending moment variation caused by reverse stretch-bending on zone III, δM_{III}, can be written as

$$\delta M_{\mathrm{III}} = \int_{R_{\mathrm{III}i}}^{R_{\mathrm{III}n}-c_{\mathrm{III}}} \left(\delta\sigma^p_{\mathrm{III}\theta} - \sigma'^p_{\mathrm{III}m\theta}\right)(r-R_m)dr + \int_{R_{\mathrm{III}n}-c_{\mathrm{III}}}^{R_{\mathrm{III}n}+c_{\mathrm{III}}} \left(\delta\sigma^e_{\mathrm{III}\theta} - \sigma'^e_{\mathrm{III}m\theta}\right)(r-R_{\mathrm{III}m})dr + \int_{R_{\mathrm{III}n}+c_{\mathrm{III}}}^{R_{\mathrm{III}o}} \left(\delta\sigma^p_{\mathrm{III}\theta} - \sigma'^p_{\mathrm{III}m\theta}\right)(r-R_{\mathrm{III}m})dr = \delta M^e_{\mathrm{III}} + \delta M^p_{\mathrm{III}} \tag{16}$$

where $\delta M^e_{\mathrm{III}}$ and $\delta M^p_{\mathrm{III}}$ are elastic and plastic bending moment variations caused by reverse stretch-bending, respectively. $\sigma'_{\mathrm{III}m\theta}{}^e$ and $\sigma'^p_{\mathrm{III}m\theta}$ are elastic and plastic tangential stresses on sheet middle surface which undergo reverse stretch-bending process, and the tangential stress on sheet middle surface, $\sigma'_{\mathrm{III}m\theta}$, *can be expressed as*

$$\sigma'_{\mathrm{III}m\theta} = \sigma_{\mathrm{III}m\theta} - Hk\left[\varepsilon_{\mathrm{III}0} + H\left(\varepsilon'_{\mathrm{III}t} + \frac{d_{\mathrm{III}}}{R_{\mathrm{III}n}}\right) - 2\frac{\sigma_{\mathrm{III}m\theta}}{E_1}\right]^n - 2\sigma_{\mathrm{III}m\theta} + H\sigma_s \tag{17}$$

where the expression of $\sigma_{\mathrm{III}m\theta}$ is similar as aforementioned $\sigma_{jm\theta}$. Thus, the tangential stress on the zone III after sheet reverse stretch-bending, $\sigma'_{\mathrm{III}\theta}$, can be written as

$$\sigma'_{\mathrm{III}\theta} = \begin{cases} \sigma_{\mathrm{III}\theta} - |\delta\sigma_{\mathrm{III}\theta}|, R_{\mathrm{III}n} \le r \le R_{\mathrm{III}o} \\ \sigma_{\mathrm{III}\theta} + |\delta\sigma_{\mathrm{III}\theta}|, R_{\mathrm{III}i} \le r \le R_{\mathrm{III}n} \end{cases} \tag{18}$$

Finally, the bending moment M'_{III} on zone III that after sheet reverse stretch-bending process can be expressed as

$$M'_{\mathrm{III}} = M_{\mathrm{III}} + \delta M_{\mathrm{III}} \tag{19}$$

5 Determination of springback parameters

Springback on zones I and V can be ignored as they basically keep flat state at loading and unloading stage, and springback is considered only at the unloading stage on zones II, III, and IV. The deformation caused by springback is equivalent to the deformation by adding a reverse-bending moment $-M_l(\phi)(l=$ II, III, IV) in corresponding region. Based on the bending-angle formula in mechanics of materials, yields

$$\frac{d\theta_l}{ds_l} = \frac{1}{R_l} = \frac{M_l(\varphi)}{E_1 I} \tag{20}$$

where $d\theta_l$ is the angle increment, ds_l is the increment of arc length, R_l is the radius of curvature, $I=t^3/12$ the inertia moment of HSLA steel plate per unit width. According to Eq. (20), the variations of angles on zones II and IV, $\delta\theta_j(j=$II, IV) (i.e., total springback angle), can be calculated as follows

$$\delta\theta_j = \int_0^{\theta} \frac{M_j(\phi)}{E_1 I} R_{jn} d\phi \tag{21}$$

Herein, define $\delta\theta_j^p$ the springback angles corresponding to the plastic strain hardening. They are considered the time-dependent springback angles in this model, yields

$$\delta\theta_j^p = \int_0^{\theta} \frac{M_j^p(\phi)}{E_1 I} R_{jn} d\phi \tag{22}$$

Table 3 Processing parameters and geometry of tool and blank

Blank holder force (kN)	Die profile radius, R_d (mm)	Punch profile radius, R_p (mm)	Length, $\bar{l}$ (mm)	Width, b (mm)	Thickness, t (mm)
8.5	5	10	700	70	0.5

Table 4 Comparison of springback parameter between Nanu and Brabie [11] and this novel model with the variation of blank holder force

Different solved methods	Blank holder force, F_p (kN)	Radius of connection between wall and bottom, $R_{\mathrm{IV}b}$ (mm)	Sidewall radius, $R_{\mathrm{III}sw}$ (mm)	Radius of connection between flange and wall, $R_{\mathrm{II}f}$ (mm)	Angle between wall and bottom, $\theta_{\mathrm{IV}b}$ (°)	Angle between flange and wall, $\theta_{\mathrm{II}f}$ (°)
Nanu and Brabie [11]	8.5	10.483	198.3	5.143	86.53	89.55
	12.5	10.465	207.5	5.132	86.72	89.95
	17.0	10.422	225.8	5.123	87.23	90.00
This novel model	8.5	10.208	250.4	5.194	86.58	100.19
	12.5	10.210	251.1	5.197	86.33	100.64
	17.0	10.214	251.9	5.200	85.83	100.95

where R_{jn} is the radius of neutral layer on *jth* zone, the superscript P represents the plastic strain hardening, therefore

$$\delta\theta_j^e = \delta\theta_j - \delta\theta_j^p = \int_0^{\theta} \frac{M_j(\phi) - M_j^p(\phi)}{E_1 I} R_{jn} d\phi \tag{23}$$

where $\delta\theta_j^e$ are considered the time-independent springback angles.

As zone III keeps a flat state before springback, the total springback angle $\delta\theta_{\mathrm{III}sw}$ is

$$\delta\theta_{\mathrm{III}sw} = \frac{M'_{\mathrm{III}}\bar{l}}{E_1 I} \tag{24}$$

where $\bar{l}$ is the length of side wall on zone III, similarly, the time-dependent springback angle caused by plastic strain hardening on zone III, is

$$\delta\theta_{\mathrm{III}sw}^p = \frac{M'^p_{\mathrm{III}}\bar{l}}{E_1 I} \tag{25}$$

where M'^p_{III} is the bending moment on zone III caused by plastic strain hardening, similar to Eq. (23), the time-independent springback angle on zone III, $\delta\theta^e_{\mathrm{III}sw}$, yields

$$\delta\theta^e_{IIIsw} = \delta\theta_{IIIsw} - \delta\theta^p_{IIIsw} = \frac{M'_{III}\bar{l} - M'^p_{III}\bar{l}}{E_1 I} \tag{26}$$

6 Results and discussion

6.1 Springback parameters

The chemical compositions of investigated HSLA steel in weight percent are summarized in Table 1 [31], also, the principal mechanical properties of HSLA steel can be seen in Table 2. The processing parameters and specific geometry of tool and blank are shown in Table 3.

Based on Eq. (20), the radius of connection between wall and flange $R_{\mathrm{II}f}$, the side wall radius $R_{\mathrm{III}sw}$ and the radius of connection between wall and bottom $R_{\mathrm{IV}b}$, can be unified as the following equation

$$R_l = \frac{E_1 t^3}{12 M_l(\varphi)} \tag{27}$$

And angle between flange and wall $\theta_{\mathrm{II}f}$ and angle between wall and bottom $\theta_{\mathrm{IV}b}$ can be defined as

$$\theta_{\mathrm{II}f} = \frac{\pi}{2} + \delta\theta_{\mathrm{II}} + \frac{\delta\theta_{\mathrm{III}sw}}{2} \tag{28a}$$

$$\theta_{\mathrm{IV}b} = \frac{\pi}{2} + \delta\theta_{\mathrm{IV}} - \frac{\delta\theta_{\mathrm{III}sw}}{2} \tag{28b}$$

Example 1 In order to validate the method presented in the paper, the comparisons of springback parameters between this paper and Nanu and Brabie's work are presented in Tables 4 and 5. In this example, all geometrical and

Table 5 Comparison of springback parameter between Nanu and Brabie [11] and this novel model with the variation of friction coefficient

Different solved methods	Friction coefficient u_d	Radius of connection between wall and bottom, $R_{\mathrm{IV}b}$ (mm)	Sidewall radius, $R_{\mathrm{III}sw}$ (mm)	Radius of connection between flange and wall, $R_{\mathrm{II}f}$ (mm)	Angle between wall and bottom, $\theta_{\mathrm{IV}b}$ (°)	Angle between flange and wall, $\theta_{\mathrm{II}f}$ (°)
Nanu and Brabie [11]	0.100	10.533	178.5	5.153	86.23	89.90
	0.144	10.482	198.0	5.145	86.55	89.95
	0.200	10.373	278.5	5.103	87.73	90.25
This novel model	0.100	10.207	249.8	5.192	86.57	100.45
	0.144	10.208	250.4	5.194	86.58	100.19
	0.200	10.210	252.2	5.197	86.04	100.85

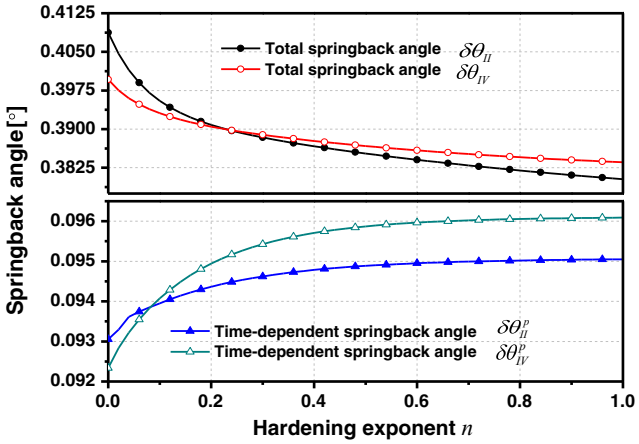

Fig. 4 The relation between the springback angle and the hardening exponent n

mechanical parameters are the same as Nanu and Brabie. From Tables 4 and 5, all the springback results are nearly the same except the radius of side wall $R_{\mathrm{III}sw}$, such parameter's error can be attributed to complicated stretch-bending and reverse stretch-bending process and is considered flat state in the process of U-bending forming, but this paper's side wall radius $R_{\mathrm{III}sw}$ is basically consistent with Nanu and Brabie's simulation result. Thus, this method is feasible and could be applied in following examples.

Example 2 This example mainly discusses the relations between the springback angles and some of parameters on zones II and IV.

Figure 4 shows the relation between the springback angles $\delta\theta_j^p$, $\delta\theta_j (j=\mathrm{II},\ \mathrm{IV})$ and the hardening exponent n. From Fig. 4, comparing with the total springback angles, the time-dependent springback behavior is significant, the ratio of $\delta\theta_j^p/\delta\theta_j$ is about 1/4. The time-dependent springback angles $\delta\theta_j^p$ increase with the increasing of hardening exponent n, but the effect of hardening exponent n on the total springback angles

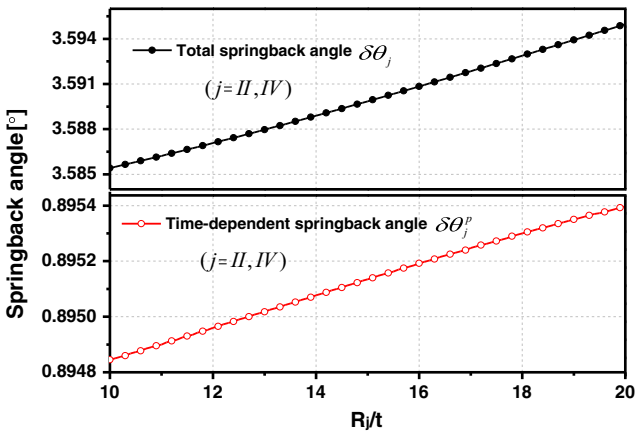

Fig. 5 The relation between the springback angle and the bending radius-thickness ratio R_j/t

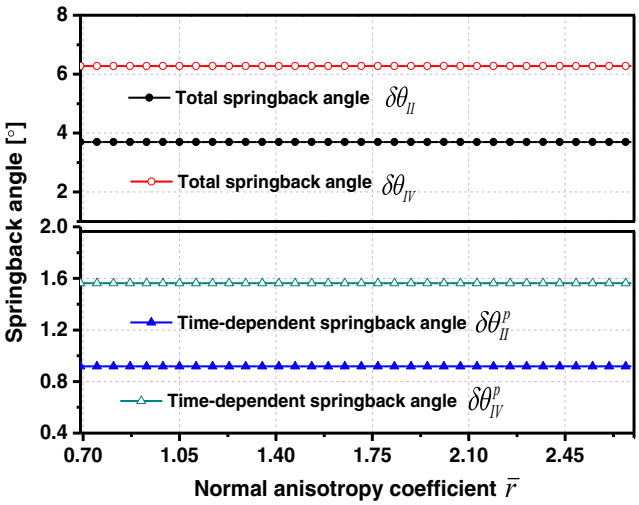

Fig. 6 The relation between the springback angle and the normal anisotropy coefficient $\bar{r}$

$\delta\theta_j$ is just opposite. And both zones' springback angles are not the same as the radii of punch and die corner differ.

Figure 5 demonstrates the relation between the springback angles $\delta\theta_j^p$, $\delta\theta_j$ and the bending radius and thickness ratio R_j/t. According to the phenomenon that springback angles $\delta\theta_j$ increase with the increasing of bending radius and thickness ratio R_j/t in Fig. 5, it can be concluded that this parameter R_j/t can be directly applied to engineering practice to avoid the springback phenomenon.

Figure 6 reflects the relation between the springback angles $\delta\theta_j^p$, $\delta\theta_j$ and the normal anisotropy coefficient $\bar{r}$. From Fig. 6, the curves of springback angles $\delta\theta_j^p$ and $\delta\theta_j$ are largely unchanged and maintain flat state with the increasing of normal anisotropy coefficient $\bar{r}$. Also, the time-dependent springback angles $\delta\theta_j^p$ occupy almost a quarter of total springback angles $\delta\theta_j$.

Figure 7 shows the relation between the springback angles $\delta\theta_j^p$, $\delta\theta_j$ and the friction coefficient u_d. The springback angles

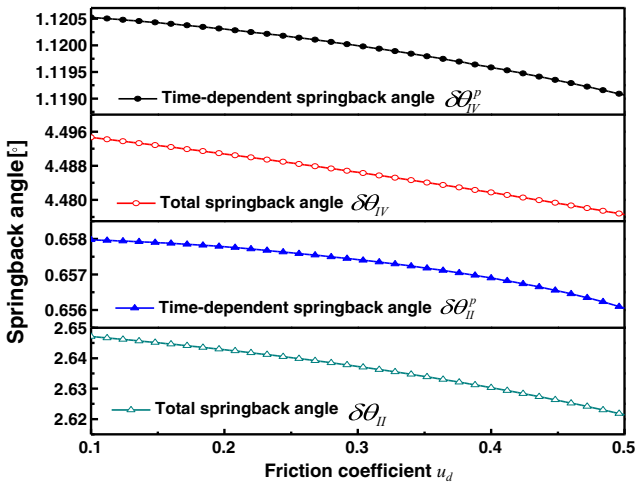

Fig. 7 The relation between the springback angle and the friction coefficient u_d

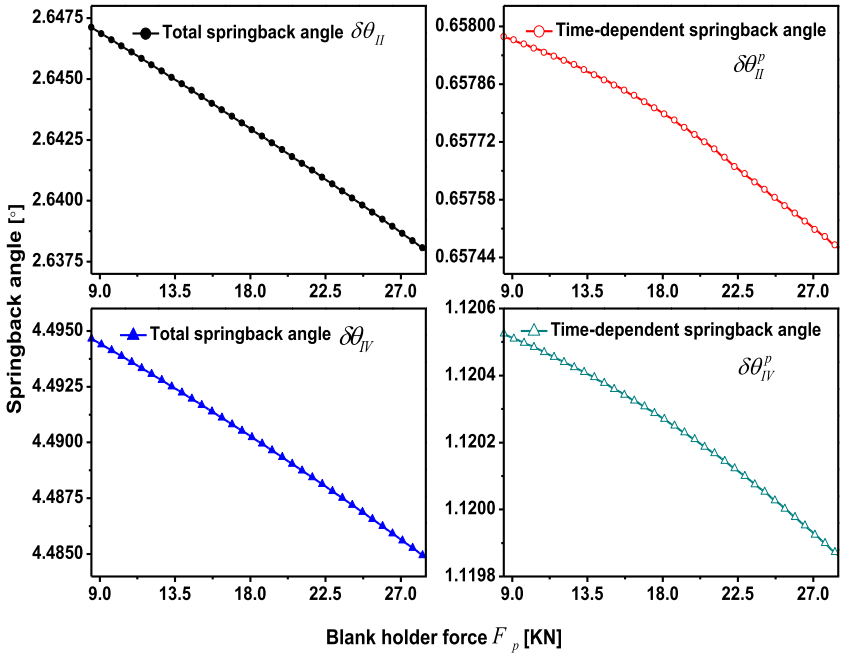

Fig. 8 The relation between the springback angle and the blank holder force F_p

$\delta\theta_j^p$ and $\delta\theta_j$ decrease with the increasing of friction coefficient u_d as the increasing of friction coefficient u_d leads to displacement of neutral axis towards layers with negative value of stress. Similarly, both two springback angles on zone IV are greater than on zone II because of respective different corner radii.

Figure 8 displays the relation between the springback angles $\delta\theta_j^p$, $\delta\theta_j$ and the blank holder force F_p. The springback angles $\delta\theta_j^p$ and $\delta\theta_j$ decrease with the increasing of blank holder force F_p as such parameter F_p modifies the neutral axis position and bending moment value in loading process, and modification that leads to variation of springback parameters after tools removing. And the declining slope of the total springback angles $\delta\theta_j$ are greater than the time-dependent springback angles $\delta\theta_j^p$ on zones II and IV. The total springback angle curves behave as straight line shapes, but the relation between time-dependent springback angles and blank holder force are parabolic curve shape.

Example 3 This example mainly discusses the curvature radius $R_{\mathrm{III}sw}$ and springback angles $\delta\theta_{\mathrm{III}sw}$, $\delta\theta_{\mathrm{III}sw}^p$ with variation of some parameters on zone III. In this example, basic parameters are as follows:

$$n = 0.163, \quad \bar{r} = 0.1, u_d = 0.1, F_p = 8.5KN \tag{29}$$

In this example, in order to investigate the effect of above-mentioned parameters in Eq. (29) on discussed curvature radius $R_{\mathrm{III}sw}$ and springback angles $\delta\theta_{\mathrm{III}sw}$ and $\delta\theta_{\mathrm{III}sw}^p$, only vary one of the parameters but other parameters maintain still.

From Table 6, the curvature radius $R_{\mathrm{III}sw}$ increases with the increasing of hardening exponent n, friction coefficient μ_d, and blank holder force F_p, but decreases with the increasing of normal coefficient $\bar{r}$. Similarly, the variations of total springback angle $\delta\theta_{\mathrm{III}sw}$ and time-dependent springback angle

Table 6 Springback results on zone III for U-bending process

Parameters	$R_{\mathrm{III}sw}$ (mm)	$\delta\theta_{\mathrm{III}sw}$(°)	$\delta\theta_{\mathrm{III}sw}^p$(°)
Hardening exponent n			
0.163	0.250412	19.836	3.95046
0.2	0.25104	20.2368	4.04536
0.3	0.252212	20.9786	4.22136
0.4	0.253031	21.4938	4.34036
0.5	0.253715	21.9208	4.4352
Normal anisotropy coefficient $\bar{r}$			
0.69	0.250412	19.836	3.95046
0.8	0.24582	16.8437	3.34278
0.9	0.241751	14.0974	2.7845
1.0	0.237802	11.3429	2.22396
1.1	0.233985	8.59121	1.663382
Friction coefficient μ_d			
0.1	0.250412	19.836	3.95046
0.2	0.252199	20.9708	4.18648
0.3	0.254245	22.2504	4.45334
0.4	0.256745	23.7863	4.77424
Blank holder force F_p (KN)			
8.5	0.250412	19.836	3.95046
12.5	0.251142	20.3011	4.04708
17	0.251952	20.8148	4.154
22	0.252826	21.365	4.26864

$\delta\theta^{p}_{\mathrm{III}sw}$ have the same variation tendency with the change of above-mentioned parameters. It can be found that the effect of aforementioned parameters on springback angles $\delta\theta^{p}_{j}$ and $\delta\theta_{j}$(j=II, IV) are just opposite when compared with the effect of such parameters on springback angles $\delta\theta_{\mathrm{III}sw}$ and $\delta\theta^{p}_{\mathrm{III}sw}$.

6.2 Stress distribution in the sheet thickness

Example 4 In order to validate the method presented in the paper, the comparison of stress distribution in sheet thickness between this paper and Nanu and Brabie's work is presented in Fig. 9. In this case, all parameters and conditions are taken the same according to reference [11]. The outer face locates at the $-t/2$ thickness level and the inner ones at the $t/2$ thickness level in global coordinate system. Namely, the outer face of zone II is the inner radius position, but the outer faces of zones III and IV are out radius position. From Fig. 9, both the curve shape and magnitude of stress distribution are approximate between this method and Nanu and Brabie's work [11].

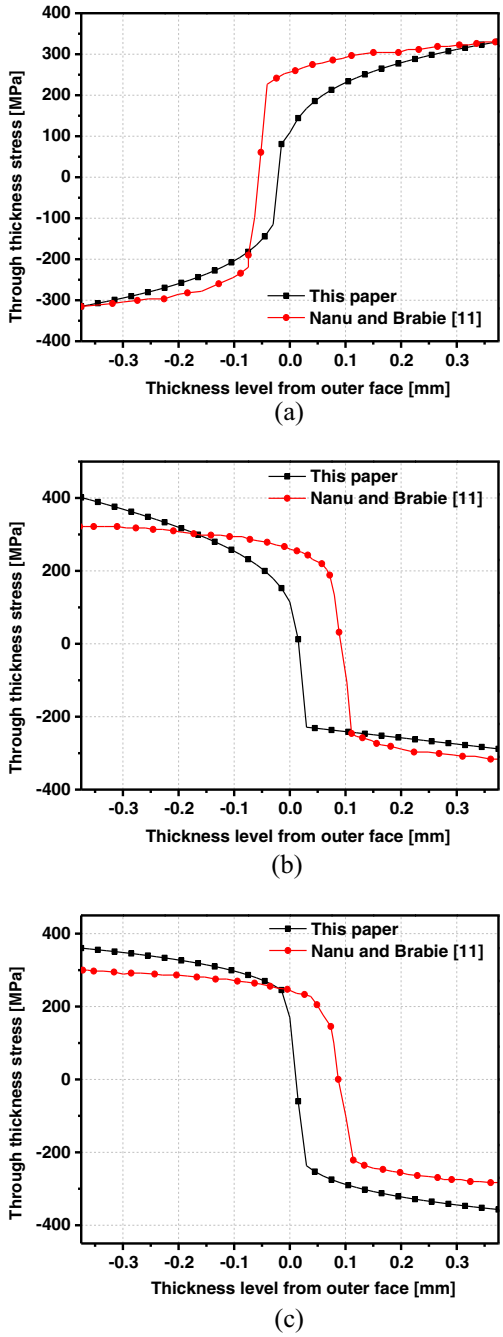

Fig. 9 Comparison of stress distribution in sheet thickness between this paper and Nanu and Brabie's work. **a** Zone II. **b** Zone III. **c** Zone IV

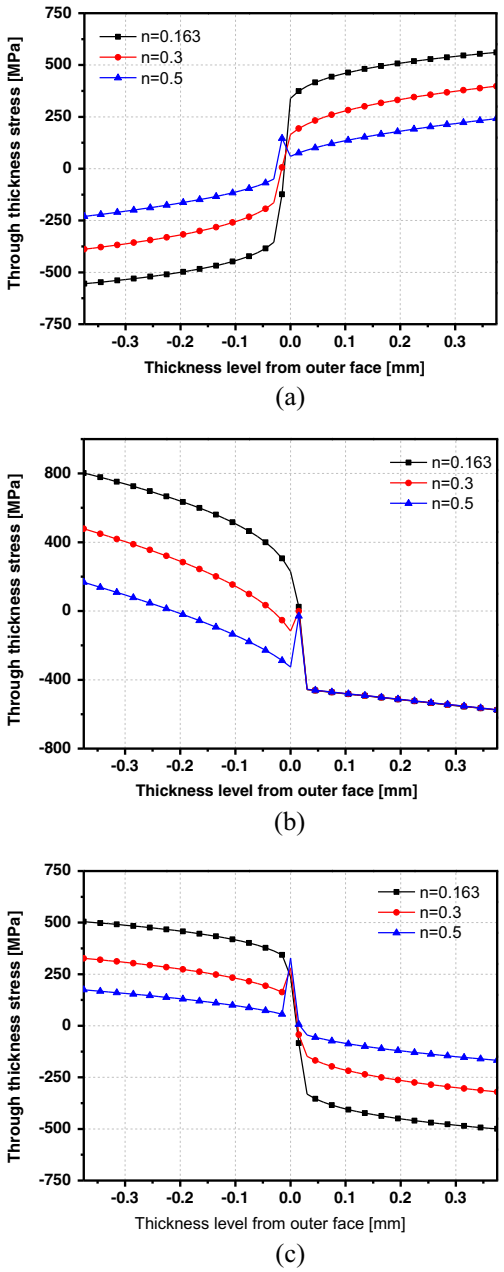

Fig. 10 Influence of hardening exponent n on the stress distribution in sheet thickness. **a** Zone II. **b** Zone III. **c** Zone IV

Example 5 This example mainly discusses the influence of hardening exponent n, friction coefficient u_d, and blank holder force F_p on the stress distribution in the sheet thickness. The stress distribution on the bending zones presents a uniform variation in sheet thickness. On the connected zone between flange and wall, the stress presents positive value on the inner face and negative value on the outer face, and on the wall and wall-bottom connected zones, the stress presents negative value on the inner face and positive value on the outer face.

Figure 10 presents the influence of hardening exponent n on the stress distribution in the sheet thickness. From Fig. 10, the stress levels of zones II and IV decrease on both outer and inner faces of sheet, but the stress level of zone III decreases only on outer face, the position of inner face does not suffer major movements.

Figure 11 shows the influence of friction coefficient u_d on the stress distribution in the sheet thickness. The increasing of friction coefficient has not a major influence on the stress levels on inner and outer faces, but it influences the neutral

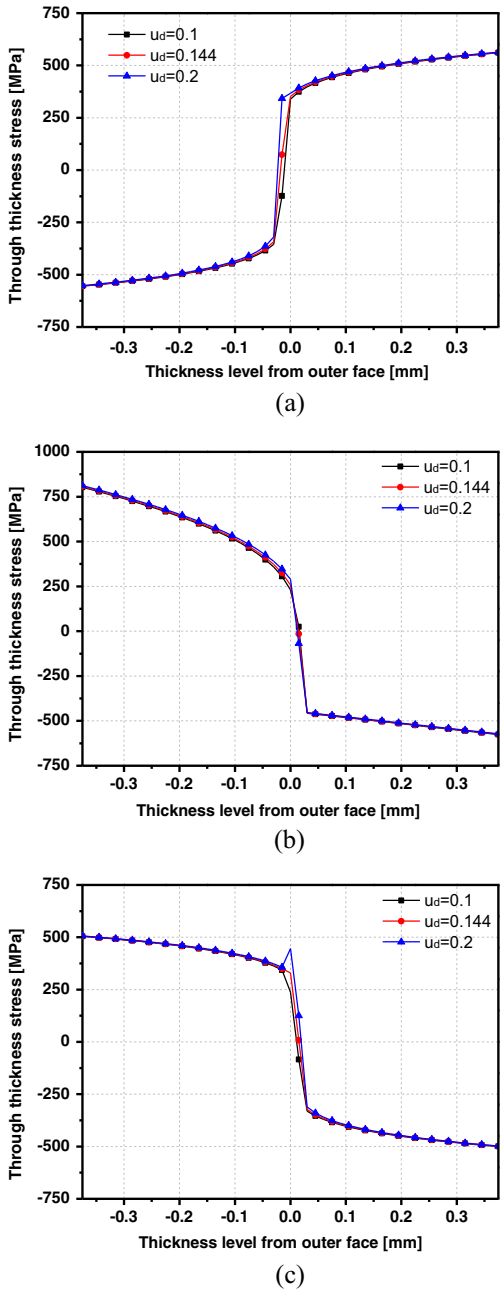

Fig. 11 Influence of friction coefficient u_d on the stress distribution in sheet thickness. **a** Zone II. **b** Zone III. **c** Zone IV

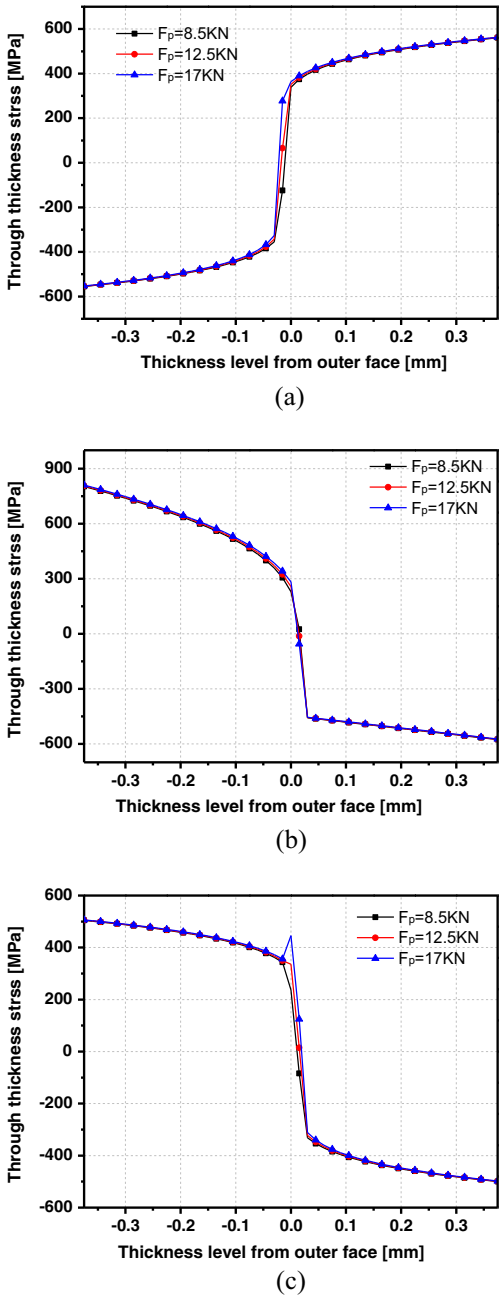

Fig. 12 Influence of blank holder force F_p on the stress distribution in sheet thickness. **a** Zone II. **b** Zone III. **c** Zone IV

axis position which moving towards layers with negative stress.

Figure 12 demonstrates the influence of blank holder force F_p on the stress distribution in the sheet thickness. As in the case of variation for friction coefficient, the increasing of blank holder force F_p has not a major influence on the stress levels for inner and outer faces, but determines the displacement of neutral axis towards layers with negative stress.

7 Conclusions

In this paper, an analytical novel model which considers an initial strain related to material's yielding stress, the combination of stretch and bending strain and isotropic hardening rule is proposed for predicting the U-bending springback and computing the stress distribution. It reveals that the time-dependent springback angles of the HSLA steel plate, $\delta\theta_l^p (l=$ II, III, IV), take up nearly a quarter of the total springback angles $\delta\theta_l$. Therefore, it is worthwhile to pay attention to such behavior in industry and research.

Both time-dependent springback angles $\delta\theta_j^p (j=$II, IV) and total springback angles $\delta\theta_j$ decrease with the increasing of friction coefficient u_d and blank holder force F_p, but increase with the increasing of bending radius and thickness ratio R_j/t, but the influence of hardening exponent n and normal anisotropy coefficient $\bar{r}$ on this two springback physical quantities have no same effect. The influence of the above-mentioned parameters on time-dependent springback angle $\delta\theta_{\mathrm{III}sw}^p$ and total springback angles $\delta\theta_{\mathrm{III}sw}$ are just opposite.

The stress levels of zones II and IV decrease on both outer and inner faces of sheet with the increasing of hardening exponent n, but the stress level of zone III decreases only on outer face, the position of inner face does not suffer major movement. The friction coefficient u_d and blank holder force F_p have no major influences on the stress level on inner and outer faces, but have influence on the position of neutral axis. The increasing of friction coefficient or blank holder force leads to the displacement of the neutral axis towards the layers with negative stress.

Acknowledgments The authors wish to thank reviewers for their valuable comments and the research is supported by the National Natural Science Foundation of China (11372105), New Century Excellent Talents Program in University (NCET-13-0184), State Key Laboratory of Advanced Design and Manufacturing for Vehicle Body (71475004), Hunan Provincial Natural Science Foundation for Creative Research Groups of China (12JJ7001) and Hunan Provincial Innovation Foundation for Postgraduate (CX2013B148).

References

1. Liu G, Lin ZQ, Xu WL, Bao YX (2002) Variable blank holder force in U-shaped part forming for eliminating springback error. J Mater Process Technol 120(1–3):259–264
2. Chang SH, Shin JM, Heo YM, Seo DG (2002) Springback characteristics of the tailor-welded strips in U-bending. J Mater Process Technol 130–131(20):14–19
3. Cho JR, Moon SJ, Moon YH, Kang SS (2003) Finite element investigation on spring-back characteristics in sheet metal U-bending process. J Mater Process Technol 141(1):109–116
4. Wang JF, Wagoner RH, Matlock DK, Barlat F (2005) Anticlastic curvature in draw-bend springback. Int J Solids Struct 42:1287–1307
5. Zhang DJ, Cui ZS, Ruan XY, Li YQ (2007) Sheet springback prediction based on non-linear combined hardening rule and Barlat89's yielding function. Comput Mater Sci 38:256–262
6. Yu ZQ, Lin ZQ (2007) Numerical analysis of dimension precision of U-shaped aluminium profile rotary stretch bending. Trans Nonferrous Metals Soc 17(3):581–585
7. Zhang DJ, Cui ZS, Ruan XY, Li YQ (2007) An analytical model for predicting springback and side wall curl of sheet after U-bending. Comput Mater Sci 38:707–715
8. Gu RJ, Yang H, Zhan M, Li H, Li HW (2008) Research on the springback of thin-walled tube NC bending based on the numerical simulation of the whole process. Comput Mater Sci 42:537–549
9. Li L, Seo YH, Heo SC, Kang BS, Kim J (2010) Numerical simulations on reducing the unloading springback with multi-step multi-point forming technology. Int J Adv Manuf Technol 48:45–61
10. Liu JG, Fu MW, Lu J, Chan WL (2011) Influence of size effect on the springback of sheet metal foils in micro-bending. Comput Mater Sci 50:2604–2614
11. Nanu N, Brabie G (2012) Analytical model for prediction of springback parameters in the case of U stretch-bending process as a function of stresses distribution in the sheet thickness. Int J Mech Sci 64:11–21
12. Lee JY, Lee JW, Lee MG, Barlat F (2012) An application of homogeneous anisotropic hardening to springback prediction in pre-strained U-draw/bending. Int J Solids Struct 49(25):3562–3572
13. Kuo CC, Lin BT (2012) Optimization of springback for AZ31 magnesium alloy sheets in the L-bending process based on the Taguchi method. Int J Adv Manuf Technol 58:161–173
14. Zhao J, Zhai RX, Qian ZP, Ma R (2013) A study on springback of profile plane stretch-bending in the loading method of pretension and moment. Int J Mech Sci 75:45–54
15. Chongthairungruang B, Uthaisangsuk V, Suranuntchai S, Jirathearanat S (2013) Springback prediction in sheet metal forming of high strength steels. Mater Des 50:253–266
16. Li G, Liu YQ, Du T, Tong HL (2014) Algorithm research and system development on geometrical springback compensation system for advanced high-strength steel parts. Int J Adv Manuf Technol 70:413–427
17. Khan MS, Coenen F, Dixon C, El-Salhi S, Penalva M, Rivero A (2015) An intelligent process model: predicting springback in single point incremental forming. Int J Adv Manuf Technol 76:2071–2082
18. Carden WD, Geng LM, Matlock DK, Wagoner RH (2002) Measurement of springback. Int J Mech Sci 44:79–101
19. Lia KP, Carden WP, Wagoner RH (2002) Simulation of springback. Int J Mech Sci 44:103–122
20. Zhu L, Beaudoin AJ, MacEwen SR, Kocks UF, Ghosh S, Castro JC, Lee JK (2004) On the time-dependent inelastic deformation of metals. AIP Conf Proc 712(1):1798

21. Wang JF, Wagoner RH, Carden WD, Matlock DK, Barlat F (2004) Creep and inelasticity in the springback of aluminum. Int J Plast 20(12):2209–2232
22. Lim H, Lee MG, Sung JH, Wagoner RH (2008) Time-dependent springback. Int J Mater Form 1:157–160
23. Lim H, Lee MG, Sung JH, Kim JH, Wagoner RH (2012) Time-dependent springback of advanced high strength steels. Int J Plast 29:42–59
24. Daxin E, Liu YF (2010) Springback and time-dependent springback of 1Cr18Ni9Ti stainless steel tubes under bending. Mater Des 31:1256–1261
25. Park T, Chung K, Ryou H, Lee MG, Wagoner RH (2010) Numerical simulation of time-dependent springback behavior for aluminum alloy 6022-T4 sheet. In: Proceedings of the 10th international conference on numerical methods in industrial forming processes dedicated to professor Zienkiewicz (1921–2009). AIP Conf Proc 1252:153–160
26. Wagoner RH, Wang JF, Li M (2006) Metalworking: sheet forming. ASM, Materials Park, OH, 14B:733–755
27. Hill R (1950) The mathematical theory of plasticity. Oxford University Press, London
28. Wagoner RH (1980) Measurement and analysis of plane-strain work hardening. Trans Inst Min Metall Sect A 11:165–175
29. Ma DJ, Ong CW, Lu J, He JW (2003) Methodology for the evaluation of yield strength and hardening behavior of metallic materials by indentation with spherical tip. J Appl Phys 94(1):288–294
30. Brammer P, Bartier O, Hernot X, Mauvoisin G, Sablin SS (2012) An alternative to the determination of the effective zero point in instrumented indentation: use of the slope of the indentation curve at indentation load values. Mater Des 40:356–363
31. Jiang HJ, Dai HL (2015) Effect of laser processing on three dimensional thermodynamic analysis for HSLA rectangular steel plates. Int J Heat Mass Transf 82:98–108